Z. Phys. C - Particles and Fields 56, 371–380 (1992)

Zeitschrift für Physik C Particles and Fields

Study of intranuclear collision effects in interactions of K^+/π^+ mesons with Al and Au nuclei at 250 GeV/c

EHS-NA22 Collaboration

N.M. Agababyan[a], I.V. Ajinenko[b], F. Botterweck[c], M. Charlet[c,*], P.V. Chliapnikov[b], E.A. De Wolf[d,**], K. Dziunikowska[e,***], A.M. Endler[f], G. Gulkanyan[a], R.Sh. Hakobyan[a], J.K. Karamyan[a], W. Kittel[c], D. Kisielewska[e,***], B.B. Levchenko[g], S.S. Megrabyan[a], K. Olkiewicz[e,***], F. Rizatdinova[g], L. Shabalina[g], F. Verbeure[d], R. Wischnewski[h]

[a] Institute of Physics, 375036 Yerevan, Armenia
[b] Institute for High Energy Physics, 142284 Serpukhov, Russian Federation
[c] University of Nijmegen and NIKHEF-H, NL-6525 ED Nijmegen, The Netherlands
[d] Department of Physics, Universitaire Instelling Antwerpen, B-2610 Wilrijk, and Interuniversity Institute for High Energies, B-1050 Brussels, Belgium
[e] Institute of Physics and Nuclear Techniques of the Academy of Mining and Metallurgy and Institute of Nuclear Physics, PL-30055 Krakow, Poland
[f] Centro Brasiliero de Pesquisas Físicas, BR-22290 Rio de Janeiro, RJ, Brazil
[g] Moscow State University, 119899 Moscow, Russian Federation
[h] Institut für Hochenergiephysik, O-1615 Berlin-Zeuthen, Federal Republic of Germany

Received 12 May 1992

Abstract. Multiplicity, inclusive, correlation and collective characteristics of multiparticle production processes in K^+ Al, K^+ Au, π^+ Al and π^+ Au interactions at 250 GeV/c are studied with the European Hybrid Spectrometer, providing high statistics and almost 4π acceptance for final state charged particles. It is shown that the proton energy spectrum practically does not depend on the target atomic weight, but the proton angular distributions reveal a strong A-dependence. In a model independent way, the average number of intranuclear collisions is extracted, and it is shown that their dominant part (60% for Al and 80% for Au) is caused by interactions of the non-leading particles produced in the target fragmentation. The multiplication ratio of the produced particles for the Au nucleus changes from $R \simeq 40$ at the smallest rapidities in the target fragmentation region, down to $R = 0.37 \pm 0.06$ at the largest rapidities in the beam fragmentation region. It is found that the average total longitudinal momentum of the charged products of the beam fragmentation depends weakly on the number of leading hadron (cluster) intranuclear collisions which are characterized by a low inelasticity coefficient $\langle k \rangle = 0.17 \pm 0.03$.

* EEC Guest Scientist
** Bevoegdverklaard Navorser NFWO, Belgium
*** Partially supported by grants from CPBP 01.06 and 01.09

1 Introduction

It is known that high energy nuclear interactions contain important information on the space-time structure and mechanisms of multiparticle production processes (see e.g. [1] for a review). Various mechanisms lead to different manifestations of the intranuclear collision effects, and thus to different predictions for the experimentally observable quantities: the multiplicity and inclusive distributions, the correlations and collective characteristics of produced particles.

The available amount of experimental data, especially on high-energy meson-nucleus interactions, suffers from low statistics or from limited acceptance, or is obtained in experiments on nuclear emulsions without identification of the nuclear target nor the charge of the secondary particles (see [1] and references cited therein).

An opportunity for a detailed study of multiparticle production processes in the meson-nucleus interaction, based on sufficiently high statistics (about 9 K events of K^+/π^+ interactions with Al and Au nuclei at 250 GeV/c) with full angular acceptance, is provided by the NA22 experiment with the european hybrid spectrometer (EHS) at CERN. The first results of this study are published in [2, 3].

In this paper we present new results on multiplicities and distributions of protons, on correlations and on col-

lective characteristics of the multiparticle production processes in K^+ Al, K^+ Au, π^+ Al and π^+ Au interactions at 250 GeV/c. The experimental procedure is shortly described in Sect. 2. The multiplicity and inclusive distributions of protons are presented in Sect. 3. Section 4 is devoted to a detailed study of the produced negative particle multiplication ratio. In Sect. 5 the charge balance of secondaries is studied and the total number of intranuclear interactions is extracted. In Sect. 6 we present data on the total longitudinal momentum of charged secondaries in the beam fragmentation region and on the nuclear stopping power. Finally, a summary is presented in Sect. 7.

2 Excperimental procedure

The experimental set-up of the EHS is described in detail in [4] and the data reduction procedures in [5, 6]. A rapid cycling bubble chamber RCBC with diameter 80 cm and filled with hydrogen, was used as vertex detector. The RCBC is equiped with two nuclear targets consisting of an aluminium and a gold foil with thickness of 2.5 mm and 0.64 mm, respectively, corresponding to 0.5% of an interaction length, and placed side by side orthogonally to the beam, 15.5 cm behind the entrance window of the chamber. Tracks of secondary charged particles are reconstructed from hits in the wire and drift chambers of the spectrometer and from measurements in the RCBC. The majority of protons with laboratory momentum less than 400 MeV/c stop inside the RCBC; their momentum is accurately determined from their range in hydrogen. The momentum resolution for all charged particles varies from (1–2)% for tracks reconstructed in the bubble chamber, and (1–2.5)% for those reconstructed in the spectrometer. For all reconstructed tracks with laboratory momentum less than about 1.2 GeV/c the ionization was estimated visually. Positive tracks with ionization compatible with the p or K/p hypotheses were taken as protons.

We used following selection criteria for the events (see details in [2]): the interaction vertex is within one of the nuclear foils; the event is satisfactorily measured and reconstructed and it is not a candidate for a quasi-elastic or coherent interaction with the nucleus. The events were weighted with a multiplicity dependent weight in order to compensate for the loss of events due to badly reconstructed tracks.

Finally, the numbers of accepted events are 1180 K^+ Al, 970 K^+ Au, 3475 π^+ Al and 2883 π^+ Au events.

The following characteristics of meson-nucleus interactions are studied:

1. the multiplicity and inclusive distributions of protons;
2. correlations between the mean multiplicities of produced hadrons and the number of "grey" protons (g-particles) i.e. protons with velocities from $\beta = 0.2$ to 0.7 or kinetic energies $T = 19$–376 MeV;
3. correlations between the π^- meson inclusive spectrum and the number n_g of g-particles; the dependence of the differential average multiplicities of π^- mesons on n_g;
4. the distributions of the total charge Q of secondary particles and
5. correlations between the total longitudinal momentum of charged secondaries in the beam fragmentation region and n_g and Q.

3 The inclusive spectra and multiplicity distributions of protons

The laboratory momentum distributions of the identified protons are shown in Fig. 1. The data for π^+ and K^+ interactions have similar shape and are combined. The distributions are corrected for ionization losses in the nuclear foils. These corrections, obtained by estimating the proton path in the foils, shift the low momentum part of the distributions noticably towards larger values with respect to the uncorrected spectra (the dotted line in Fig. 1, where the momentum interval for g-particles $192 < p < 920$ MeV/c is marked by arrows).

The proton kinetic energy (Fig. 2) and the momentum square distributions can be fitted by the sum of two exponentials (for the regions $T > 40$ MeV and $p^2 >$

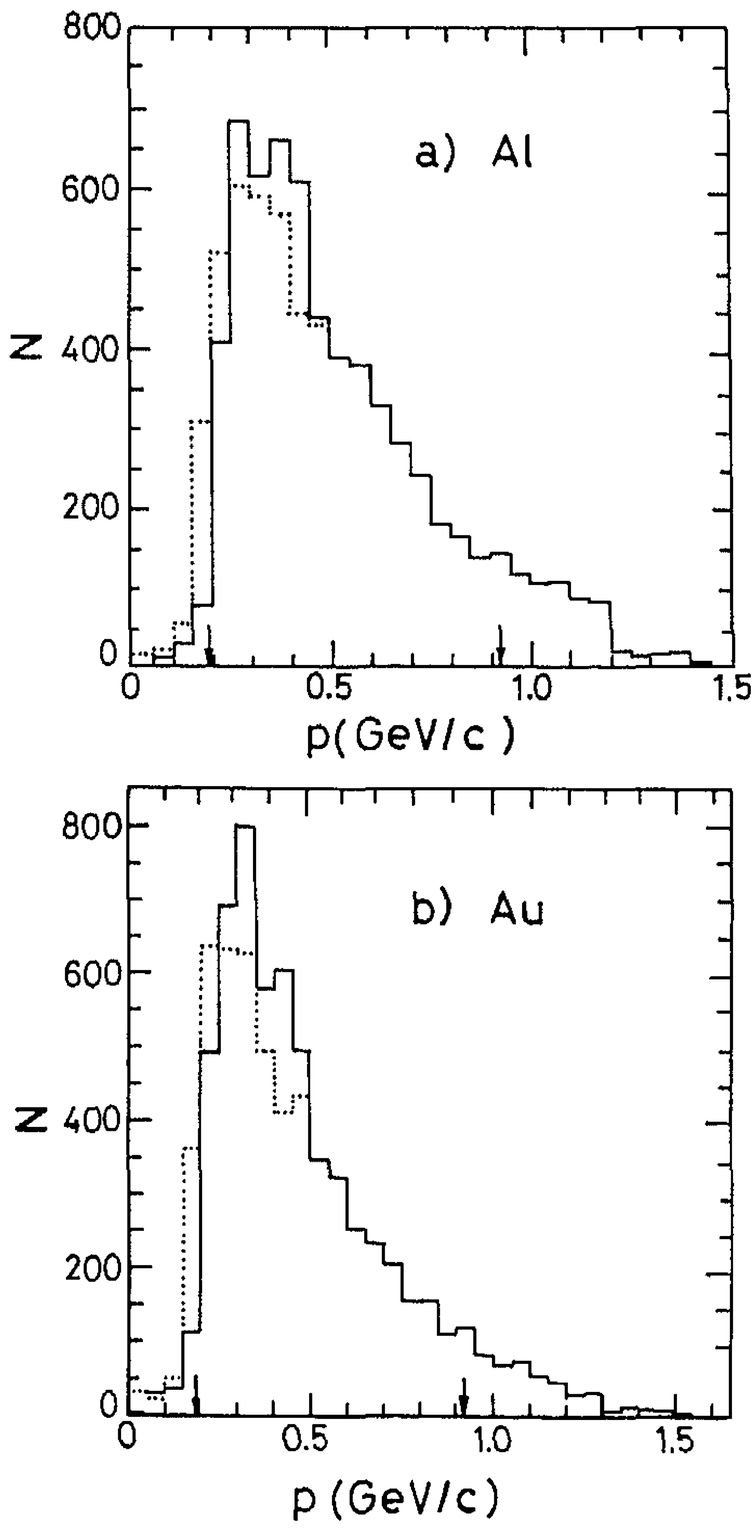

Fig. 1a,b. The momentum distributions of identified protons, normalized to the total number of particles. The dashed histogram is the uncorrected spectrum

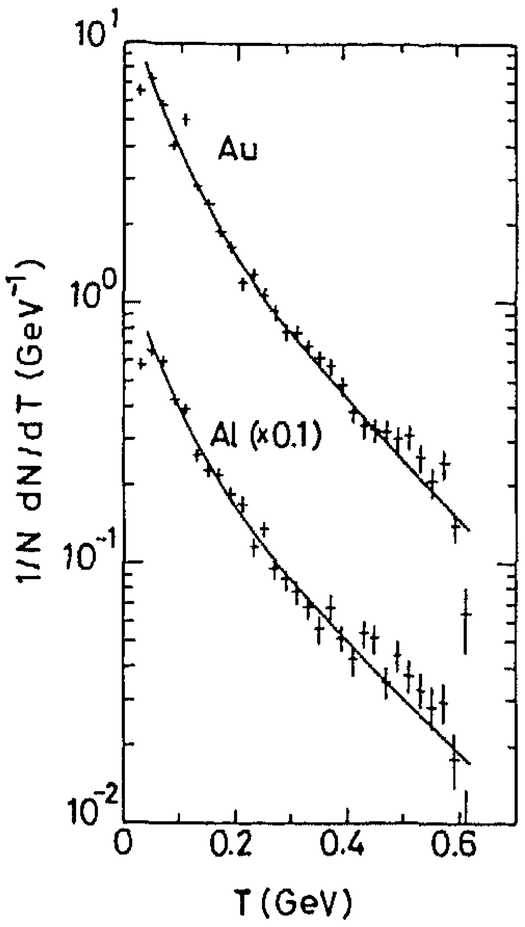

Fig. 2. The energy distributions of the identified protons. The curves are the fit results (see text)

$0.04\,(\mathrm{GeV/c})^2$, respectively:

$$\frac{1}{N}\frac{\mathrm{d}N}{\mathrm{d}T}=A_1\exp(-T/T_1)+A_2\exp(-T/T_2), \qquad (1a)$$

$$\frac{1}{N}\frac{\mathrm{d}N}{\mathrm{d}p^2}=B_1\exp(-p^2(p_1^2)+B_2\exp(-p^2/p_2^2). \qquad (1b)$$

The fitted parameters are presented in Table 1; one can see that the shape of the spectrum practically does not depend on the target mass. The first term in (1a) (with slope $T_1\simeq 190\leftrightarrow 200$ MeV), probably refers to the "direct" recoiling protons, and the second one (with slope $T_2\simeq 55\leftrightarrow 58$ MeV) may reflect the secondary interaction processes within the nucleus.

Figure 3 shows the angular distributions of the g-particles (Fig. 3a) and the recoil protons (Fig. 3b) with energies $T\geqq 40$ MeV; the lower bound of $T\geqq 40$ MeV is choosen in order to suppress the contamination from nuclear "evaporation" products. The angle θ is the angle between the beam direction and the proton. The distributions are corrected for the loss of low energy protons stopping in the foil or having a very short range in the hydrogen. The π^+ and K^+ data are of similar form and are combined. Some loss of protons near $\theta\sim 90°$ can be explained by absorption in the foils or bad reconstruction

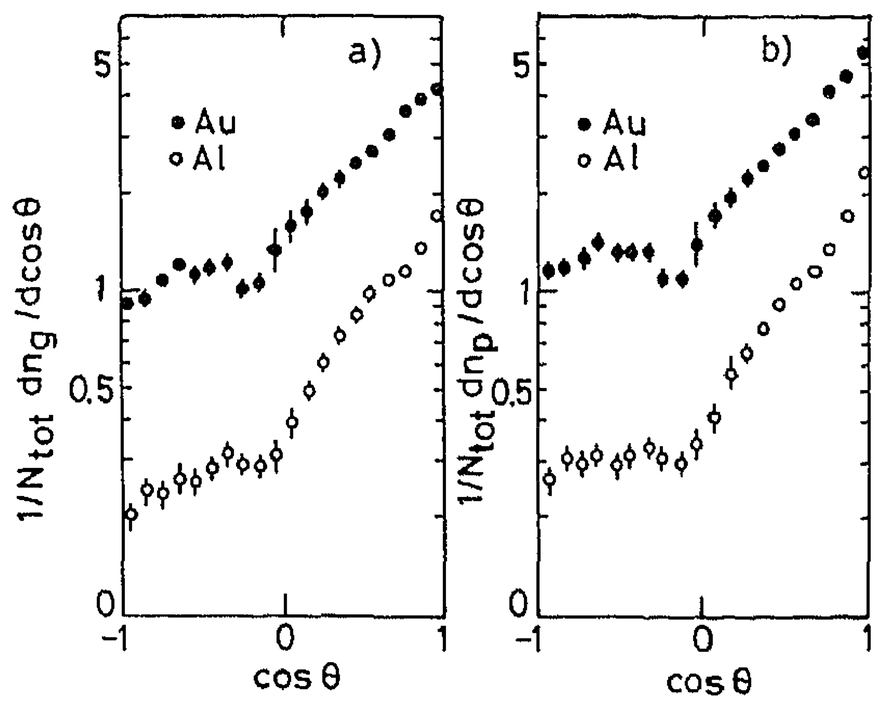

Fig. 3a, b. The angular distributions of the g-particles and recoil protons

of tracks going almost parallel to the foil; this loss is estimated to be $\leqq 5\%$ for all g-particles for both nuclei. As one can see from Fig. 3, the angular distribution for the heavier nucleus is significantly shifted towards larger angles. The A-dependence of the average differential multiplicity $\langle n_r(\cos\theta)\rangle$ of recoil protons in different angular intervals (with the parametrization $\sim A^\alpha$, A being the atomic weight of nucleus) is shown in Table 2. The exponent α increases with θ in the forward hemisphere, from $\alpha=0.42\pm 0.02$ at very small angles ($0.9<\cos\theta<1$) to 0.63 ± 0.04 at $\cos\theta=0.1\leftrightarrow 0.3$. In the backward hemisphere, α is independent of θ within errors. The average value of the exponent is $\alpha=0.73\pm 0.03$ in the interval $-1<\cos\theta<-0.3$.

The observed A-dependence of the proton yield at all angles is much stronger than that for the average number of intranuclear collisions of the leading hadron (or had-

Table 2. Exponents α in the parametrization $\sigma\sim A^\alpha$ in different angular regions for the protons

$\cos\theta$	α
$-1.0\leftrightarrow -0.3$	0.73 ± 0.03
$-0.3\leftrightarrow 0.1$	0.68 ± 0.04
$0.1\leftrightarrow 0.3$	0.63 ± 0.04
$0.3\leftrightarrow 0.5$	0.56 ± 0.04
$0.5\leftrightarrow 0.6$	0.52 ± 0.03
$0.6\leftrightarrow 0.7$	0.53 ± 0.03
$0.7\leftrightarrow 0.8$	0.55 ± 0.03
$0.8\leftrightarrow 0.9$	0.49 ± 0.03
$0.9\leftrightarrow 1.0$	0.42 ± 0.02

Table 1. Results of fits of the distributions of kinetic energy and momentum squared of protons to a sum of two exponentials (1)

	A_1 $(\mathrm{GeV})^{-1}$	T_1 (GeV)	A_2 $(\mathrm{GeV})^{-1}$	T_2 (GeV)
(K^+/π^+) Al	3.56 ± 0.78	0.204 ± 0.020	9.64 ± 1.00	0.058 ± 0.010
(K^+/π^+) Au	3.53 ± 0.56	0.189 ± 0.012	11.44 ± 0.99	0.055 ± 0.006

	B_1 $(\mathrm{GeV/c})^{-2}$	p_1^2 $(\mathrm{GeV/c})^2$	B_2 $(\mathrm{GeV/c})^{-2}$	p_2^2 $(\mathrm{GeV})^2$
(K^+/π^+) Al	0.68 ± 0.21	0.672 ± 0.117	4.38 ± 0.20	0.166 ± 0.014
(K^+/π^+) Au	0.76 ± 0.16	0.559 ± 0.057	5.03 ± 0.18	0.151 ± 0.009

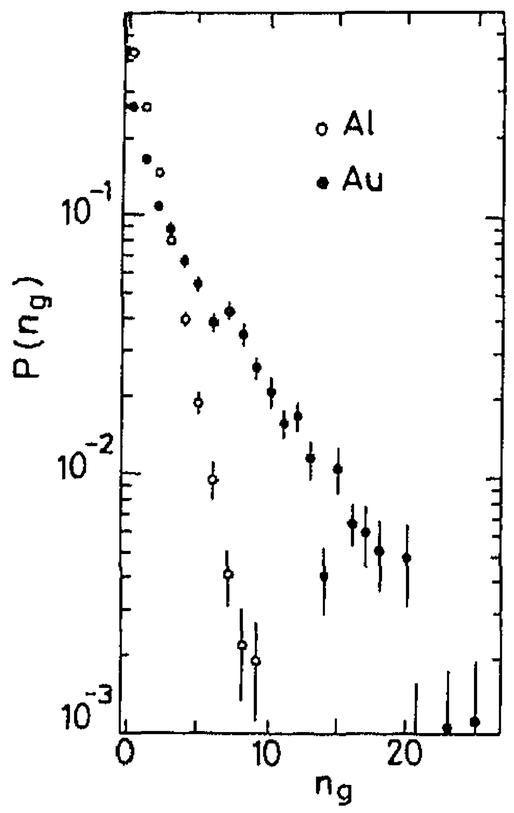

Fig. 4. The multiplicity distributions of the *g*-particles

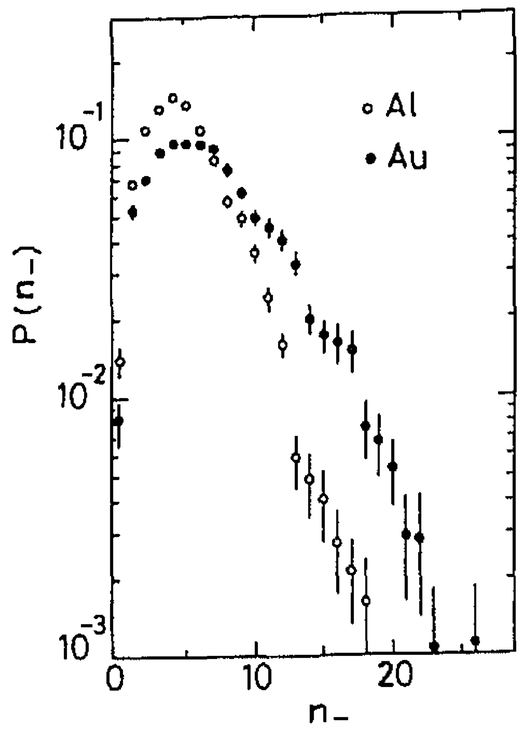

Fig. 5. The multiplicity distributions of π^- mesons

ron cluster); therefore most of the protons are produced in intranuclear collisions of the secondary, non-leading, particles (see Sect. 5 below).

In Fig. 4 the multiplicity distributions of "grey" protons are shown; the average multiplicities of "grey" and of all identified protons are presented in Table 3.

4 The particle multplication ratio

A commonly adopted measure of the particle multiplication in the interaction with a nucleus is the ratio

$$R = \langle n \rangle_{hA} / \langle n \rangle_{hp},$$

where $\langle n \rangle_{hA}$ and $\langle n \rangle_{hp}$ are the average charge multiplicities of produced particles in collisions with a nucleus and a proton, respectively.

The average multiplicities of the various types of secondary particles (all charges, negative and positive hadrons, identified protons, *g*-particles) in K^+ Al, K^+ Au, π^+ Al and π^+ Au interactions are presented in Table 3. The NA22 data [5, 7] on average multiplicities in $K^+ p$ and $\pi^+ p$ inelastic and non-single diffractive collisions at 250 GeV/c are also given.

The multiplicity distributions of negative particles, the overwhelming part of which are π^-'s, are shown in Fig. 5 and their average multiplication ratio R_- is plotted in Fig. 6 versus the average number of leading hadron in-

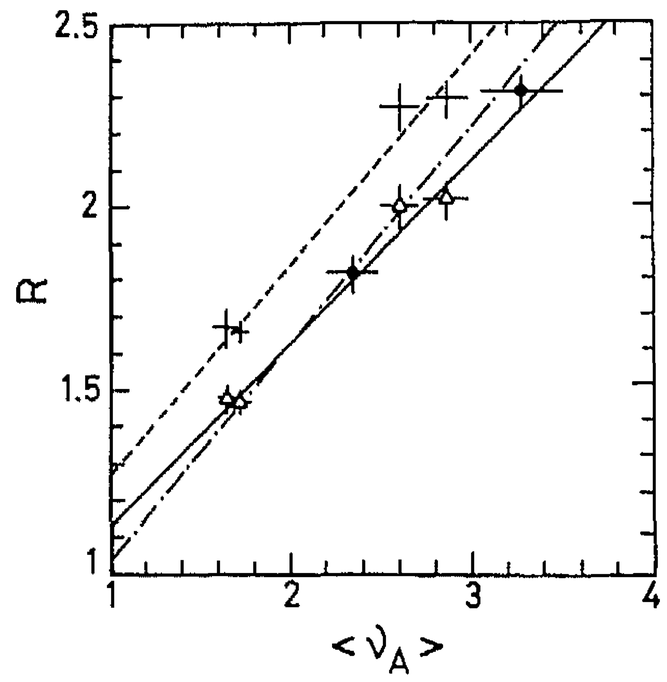

Fig. 6. The average multiplication ratio R_- versus the average number of leading hadron (cluster) inelastic collisions. Crosses (triangles) are calculated using $\langle n_- \rangle_{hp}$ from inelastic (non-single diffractive) interactions. The solid and dashed lines are the fit results (see text). The data of [9] (circles) and [10] (dot-dashed line) are also shown

elastic collisions with the nucleons inside the nucleus (see Table 4, fourth column)

$$\langle \nu_A \rangle = A \frac{\sigma_{hp}^{in}}{\sigma_{hA}^{a}}, \tag{2}$$

calculated in the assumption that the leading hadron (cluster) undergoes multiple inelastic scatterings with the "usual" hadron-nucleus cross section σ_{hp}^{in} with

Table 3. Average multiplicities $\langle n \rangle$ of charged particles, $\langle n_- \rangle$ of negative and $\langle n_+ \rangle$ of positive particles, $\langle n_p \rangle$ of protons and $\langle n_g \rangle$ of *g*-particles

	$\langle n \rangle$	$\langle n_- \rangle$	$\langle n_+ \rangle$	$\langle n_p \rangle$	$\langle n_g \rangle$
K^+ Al	13.61 ± 0.23	5.20 ± 0.10	8.41 ± 0.14	1.41 ± 0.05	1.20 ± 0.05
K^+ Au	20.96 ± 0.47	7.05 ± 0.15	13.91 ± 0.35	4.16 ± 0.17	3.65 ± 0.15
$K^+ p$ (inel)	8.22 ± 0.12	3.11 ± 0.06	5.11 ± 0.06		
$K^+ p$ (non-diff)	9.04 ± 0.14	3.52 ± 0.07	5.52 ± 0.07		
π^+ Al	13.83 ± 0.14	5.25 ± 0.06	8.58 ± 0.09	1.37 ± 0.03	1.18 ± 0.03
π^+ Au	21.88 ± 0.28	7.22 ± 0.09	14.66 ± 0.20	4.29 ± 0.10	3.74 ± 0.09
$\pi^+ p$ (inel)	8.32 ± 0.10	3.16 ± 0.05	5.16 ± 0.05		
$\pi^+ p$ (non-diff)	9.16 ± 0.12	3.58 ± 0.06	5.58 ± 0.06		

Table 4. Average total charge $\langle Q \rangle$, average total number of intranuclear collisions $\langle \nu_T \rangle$, of leading hadron collisions $\langle \nu_A \rangle$ and of cascade collisions $\langle \nu_K \rangle$

	$\langle Q \rangle$	$\langle \nu_T \rangle$	$\langle \nu_A \rangle$	$\langle \nu_K \rangle$
K^+ Al	3.07 ± 0.06	4.30 ± 0.12	1.65 ± 0.06	2.65 ± 0.10
π^+ Al	3.22 ± 0.04	4.61 ± 0.08	1.73 ± 0.05	2.88 ± 0.06
K^+ Au	6.15 ± 0.17	12.84 ± 0.42	2.61 ± 0.11	10.23 ± 0.41
π^+ Au	6.75 ± 0.11	14.34 ± 0.27	2.86 ± 0.12	11.48 ± 0.24

$\sigma^{\text{in}}_{K^+p} = 17.72 \pm 0.11$ mb and $\sigma^{\text{in}}_{\pi^+p} = 20.94 \pm 0.12$ mb [5]. In (2) σ^a_{hA} is the absorption cross section of the hadron-nucleus interaction (at 250 GeV/c, $\sigma^a_{K^+\text{Al}} = 290 \pm 10$ mb, $\sigma^a_{\pi^+\text{Al}} = 327 \pm 10$ mb, $\sigma^a_{K^+\text{Au}} = 1340 \pm 60$ mb, $\sigma^a_{\pi^+\text{Au}} = 1440 \pm 60$ mb [8]).

Note that our data selection procedure excludes a part of the single-diffractive scattering of the incident hadron on the intranuclear nucleons. Therefore, in calculating the ratio R_-, we use two different values of $\langle n_- \rangle_{hp}$ corresponding to the inelastic and the non-single diffractive interactions (see Table 3). Our data can be fitted by expression

$$R_- = a + b\langle \nu_A \rangle , \tag{3}$$

with $a = 0.70 \pm 0.14$ and $b = 0.57 \pm 0.07$ for the former case (see crosses and dashed line in Fig. 6) and $a = 0.64 \pm 0.12$ and $b = 0.50 \pm 0.06$ for the latter (triangles and solid line in Fig. 6). The quoted errors include the uncertainties in R_- and $\langle \nu_A \rangle$. Figure 6 also shows data on the multiplication ratio R for negative particles produced in p Ar and p Xe interactions at 200 GeV/c [9] (full circles), and for relativistic charged particles ($\beta > 0.85$) produced at laboratory angles $0 < \theta < 110°$ in the interactions of $\pi^\pm$, $K^\pm$, p, $\bar{p}$ with different nuclei at 50–200 GeV/c [10] (the dot-dashed line with parameters $a = 0.45 \pm 0.02$ and $b = 0.59 \pm 0.01$).

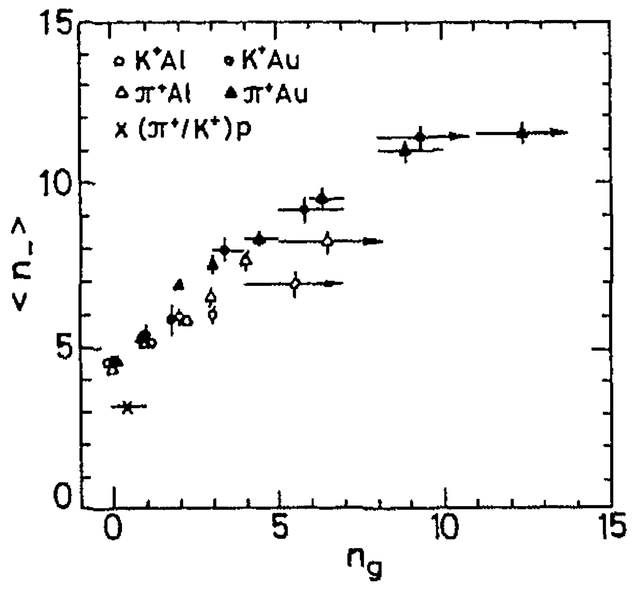

Fig. 7. The dependence of $\langle n_- \rangle$ on n_g

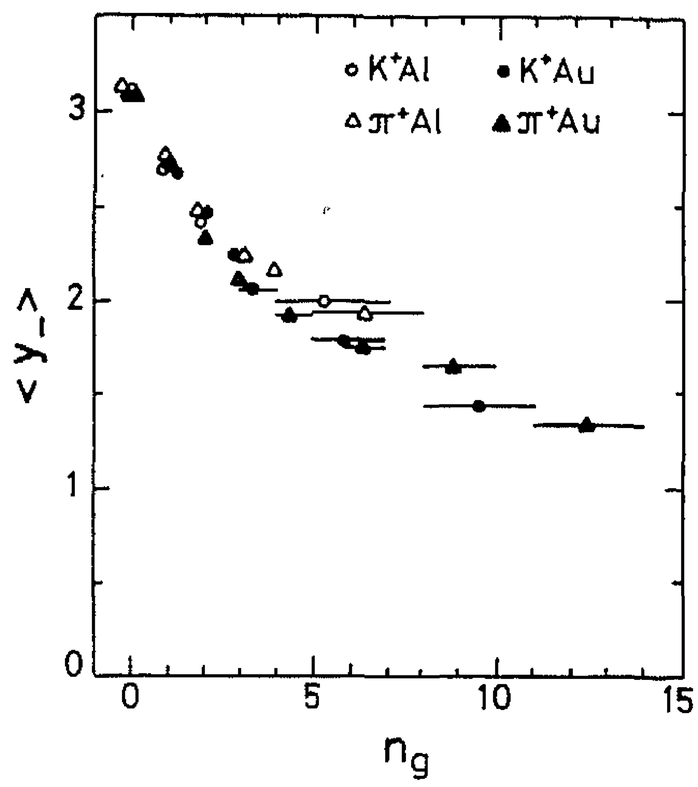

Fig. 8. The dependence of the average rapidity $\langle y_{\pi^-} \rangle$ on n_g

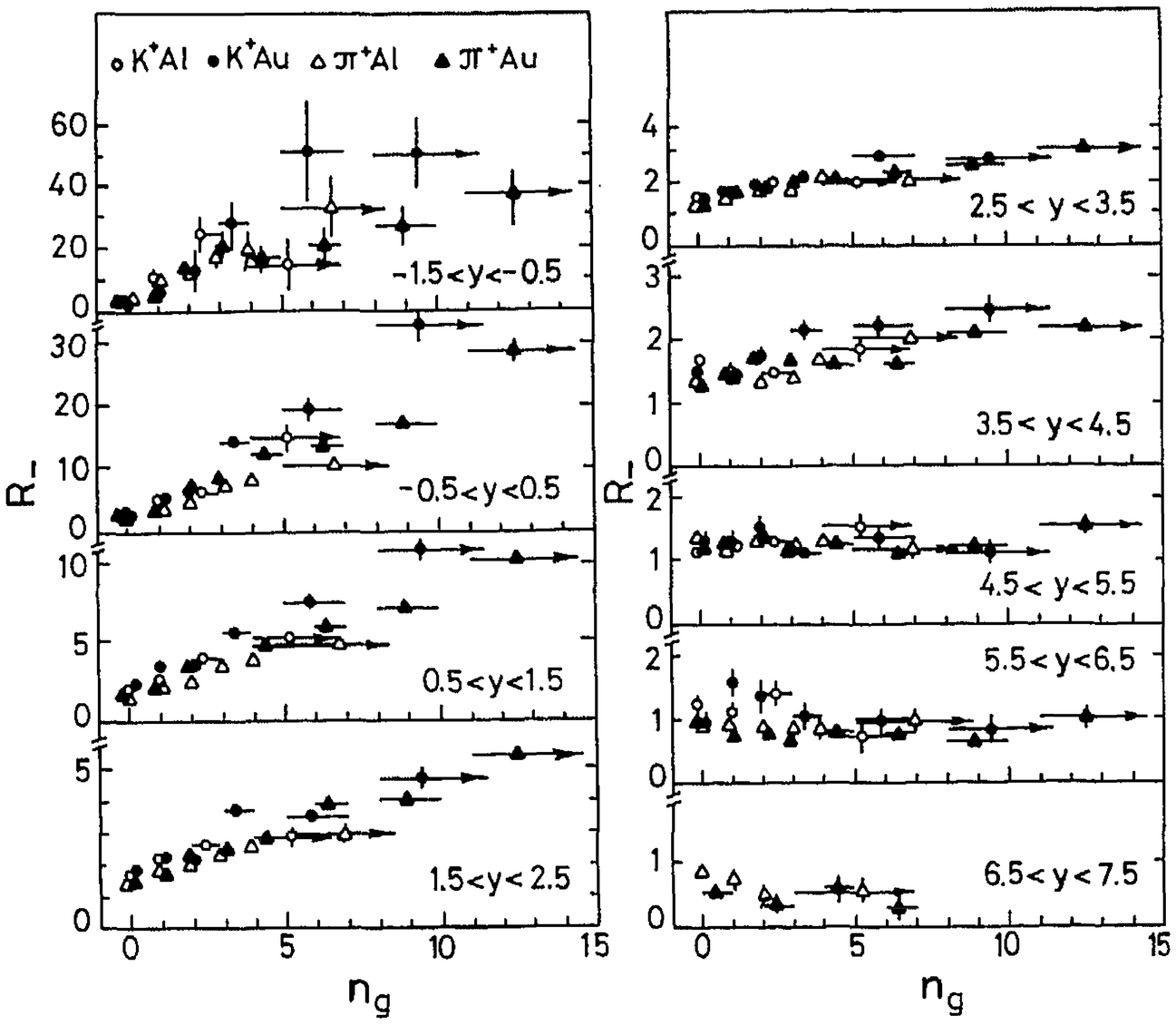

Fig. 9. The n_g – dependence of R_- for different rapidity intervals

In Fig. 7 the dependence of the average negative multiplicity $\langle n_- \rangle$ on n_g is shown. For peripheral collisions ($n_g = 0$ or 1), the multiplication factor R_- is about $1.4 \leftrightarrow 1.7$ and depends weakly on the target mass; for central collisions (at the highest values of n_g) the ratio R_- reaches up to 2.6 for Al and 3.5 for Au.

The n_g-dependence of R_- is very different for various rapidity intervals of the produced particles and shifts towards lower values as n_g increases, both for Al and Au nuclei (see the dependence of the average laboratory rapidity $\langle y_{\pi^-} \rangle$ on n_g in Fig. 8). Figure 9 presents the n_g-dependence of R_- for different rapidity intervals. In the target fragmentation region ($y < 0.5$) R_- is large and depends strongly on n_g, reaching at the smallest rapidities $-1.5 < y < -0.5$ values up to about 30–50 for central collisions. The large multiplication ratio in the target fragmentation region can not be explained only by multiple collisions of the leading hadron (with average numbers: $\langle \nu_{Al} \rangle = 1.73$ and $\langle \nu_{Au} \rangle = 2.86$ for π^+ nucleus interactions, see Table 4) and testifies about the important role of secondary collisions of the produced particles, leading to the softening of the spectra; as will be shown below in Sect. 5, $\langle \nu_A \rangle$ constitutes only a small part of the average number of all intranuclear collisions.

When approaching the central and then the beam fragmentation regions, R_- continuously decreases and becomes even less than one at the largest rapidities; at $y > 6.5$, $R_- = 0.37 \pm 0.06$ for π^+ Au and 0.71 ± 0.08 for π^+ Al interactions averaged over n_g. The dependence on n_g weakens and practically disappears in the beam fragmentation region $y > 4.5$.

5 The total number of intranuclear collisions

The full reconstruction of all secondary charged particles in the experiment allows to determine the average total number of the intranuclear collisions $\langle \nu_T \rangle$, in a model-independent way, using the charge balance of the secondary particles. Indeed, each intranuclear collision increases the total charge of secondaries on average by (Z/A), where Z is the atomic number of the nucleus. Thus, the average total charge $\langle Q \rangle$ of the final state particles is connected to $\langle \nu_T \rangle$ by the relation

$$\langle \nu_T \rangle = \frac{A}{Z} (\langle Q \rangle - q_{\text{in}}), \tag{4}$$

where $q_{\text{in}} = +1$ is the charge of the incident particle. The $\langle Q \rangle$ is determined experimentally as $\langle Q \rangle = \langle n'_+ \rangle - \langle n_- \rangle$, where $\langle n'_+ \rangle$ is the mean multiplicity of positive particles, from which the low energy ("evaporation") protons with energies $T_p < 40$ MeV are excluded, as they are not directly connected with intranuclear collisions. The probability distributions for Q are shown in Fig. 10. About 4–5% of the events having $Q \leqq 0$, i.e. less than the minimal expected value of $Q_{\text{min}} = 1$ for positive meson-nucleus interactions, correspond to relatively peripheral interactions in which one or more recoil protons acquire energies $T < 40$ MeV and are excluded from charge balance. The more probable value of Q for these events is

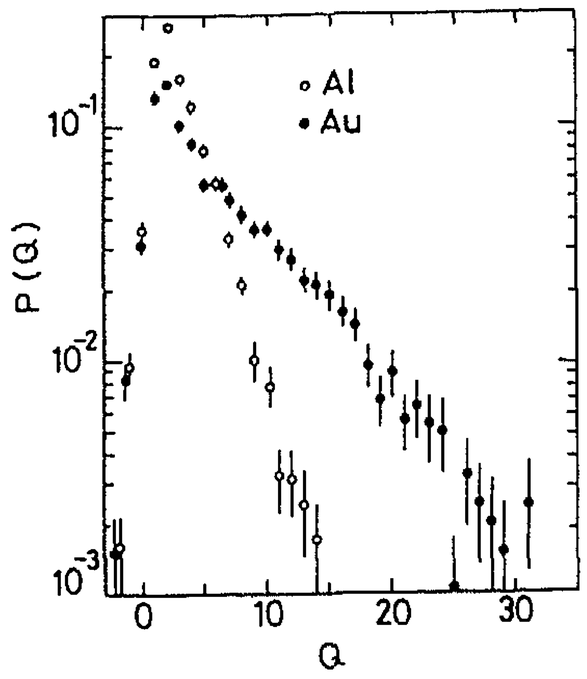

Fig. 10. The distribution of the total charge Q of secondary particles

$Q = 1$ or 2, corresponding to interactions on a neutron or proton, respectively. This is taken into account in the calculation of the average values $\langle Q \rangle$, presented in Table 4, by giving the $Q \leqq 0$ randomly a value of 1 or 2. In Table 4 we also present the average number of leading hadron (cluster) intranuclear collisions $\langle \nu_A \rangle$ (see (2)) and the average number of non-leading-particle intranuclear collisions

$$\langle \nu_K \rangle = \langle \nu_T \rangle - \langle \nu_A \rangle .$$

Once can see that $\langle \nu_A \rangle$ is only a small part of the total number of intranuclear collisions: about 40% for Al and about 20% for Au nuclei.

According to several models (see e.g. [11]), the major role in the intranuclear collisions is played by the target fragmentation products, created in the multiple interactions of the leading hadron (cluster). In the framework of Glauber theory, the mean number of intranuclear collisions in the interaction of hadron h with nucleus A is given by the expression

$$\langle \nu_T \rangle = \frac{A}{N(0, \sigma_{hN})} + \frac{A \sigma_{hN}^{\text{in}}}{N(0, \sigma_{hN}) \sigma_{hN}} \times \left\langle \sum_i m_i \left(1 - \frac{N(0, \sigma_i)}{A} \right) \right\rangle, \tag{5}$$

where

$$\sigma N(0, \sigma) = \int [1 - e^{-\sigma T(\mathbf{b})}] \, d^2 b, \tag{6}$$

with

$T(\mathbf{b}) = \int \rho(\mathbf{b}, z) \, dz$,

$\rho(\mathbf{b}, z)$ the one-particle nuclear density,
σ_{hN}^{in} is the inelastic hN cross section, and

$\sigma_{hN} = \sigma_{hN}^{\text{in}} + \Delta \sigma_{hN}^{\text{el}}(|t| > t_{\text{min}})$,

where $\Delta \sigma_{hN}^{\text{el}}(|t| > t_{\text{min}})$ is the fraction of the elastic hN cross section with momentum transfer $|t| \geqq t_{\text{min}} \approx 2 m_N T_{\text{min}}$, where $T_{\text{min}} = 40$ MeV, the minimal energy of the recoil proton.

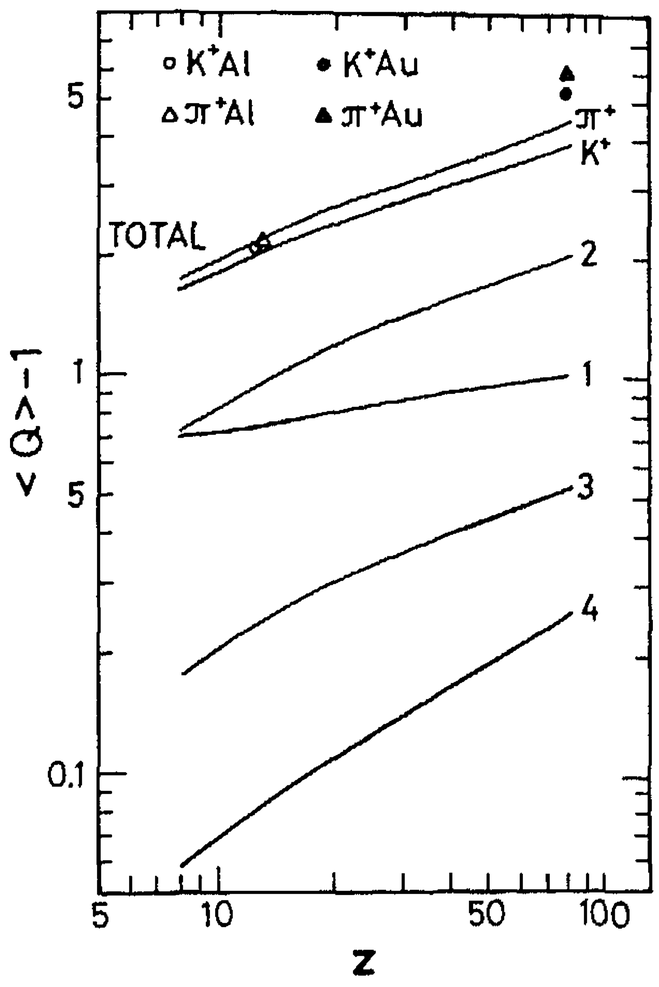

Fig. 11. Comparison of the data on $\langle Q \rangle$ with theoretical predictions

The first term in (5) is the average number of leading hadron (cluster) intranuclear collisions. In the charge balance of $\langle Q \rangle$ its value is multiplied by (Z/A) (curve 1 for K^+ nucleus interactions in Fig. 11).

The second term in (5) is the average number of intranuclear collisions of the target fragmentation products, created in the inelastic collisions of the leading hadron (or cluster) within the nucleus. The number of i-th type of the secondary hadrons h_i in the "elementary" hadron-nucleon interaction is m_i, and σ_i is the interaction cross section (either inelastic or elastic with $|t| \geqq t_{\min}$) of the hadron h_i with a nucleon.

We consider three fractions of the second term of (5):

● the comparatively low energy pions ($p_\pi < 2$–3 GeV/c). In order to calculate this fraction we use the NA22 and other experimental data [6, 12]. The mean multiplicities $\bar{m}_\pi(p_\pi)$ of low energy pions (π^+, π^-, π^0) in hN interactions at sufficiently high energies (> 100 GeV) and their mean cross sections $\bar{\sigma}_\pi = \bar{\sigma}_{\pi N}(p_\pi)$ (with $|t| > t_{\min}$) are presented in Table 5. The calculated fraction $\langle \nu_\pi \rangle$ in the second term is equal to $\langle \nu_\pi \rangle_{\mathrm{Al}} \approx 2.0$ for K^+ Al and $\langle \nu_\pi \rangle_{\mathrm{Au}} \approx 4.9$ for K^+ Au interactions, yielding the main contribution to $\langle \nu_T \rangle$.

In the charge balance of $\langle Q \rangle$ they are multiplied by (Z/A) (curve 2 in Fig. 11).

● The recoil nucleons (with $T_N > 2\,T_{\min} = 80$ MeV) produced in the inelastic interactions of the leading hadron (cluster).

The mean multiplicities $\bar{m}_N(x_F)$ of nucleons in high energy inelastic hN-interactions and their mean cross sections $\bar{\sigma}_N = \bar{\sigma}_{NN}(x_F)$ (with $|t| > t_{\min}$) versus Feynman-x_F are presented in Table 6.

The calculated fraction $\langle \nu_N \rangle$ in the second term of (5) is $\langle \nu_N \rangle_{\mathrm{Al}} \approx 0.5$ for K^+ Al and $\langle \nu_N \rangle_{\mathrm{Au}} \approx 1.33$ for K^+ Au interactions. In the charge balance of $\langle Q \rangle$ they are multiplied by Z/A (curve 3 in Fig. 11).

● A rough estimation is also made for the process of absorption of slow pions ($p_\pi \sim 0.2$–0.4 GeV/c) on quasideuteron pairs ($\pi'' d'' \to NN$).

When a pion interacts with nucleons in the nuclear matter, there is some probability for its absorption by a correlated pair of nucleons or quasideuteron pair. We assume that this probability is proportional to the ratio (N_d/A) of the quasideuteron effective number N_d and the nucleon number A, and to the ratio $\sigma(\pi'' d'' \to NN)/\sigma_i$, where $\sigma(\pi'' d'' \to NN)$ is the cross section of the free deuteron desintegration and $\sigma_i = \sigma_{\pi N}$ is the pion-nucleon cross section (with $|t| > t_{\min}$). We use $\langle \sigma(\pi'' d'' \to NN)/\sigma_{\pi N} \rangle \approx 0.13$ [12] (for $p_\pi \sim 0.2$–0.4 GeV/c) and $N_d/A = A^{0.147}$ [13].

$$\langle \nu_{\mathrm{abs}} \rangle = \frac{A \cdot \sigma_{hN}^{\mathrm{in}}}{N(0, \sigma_{hN}) \cdot \sigma_{hN}} \bar{m}_\pi \left(1 - \frac{N(0, \bar{\sigma}_i)}{A}\right) \times \left\langle \frac{\sigma(\pi'' d'' \to NN)}{\sigma_i} \right\rangle \frac{N_d}{A}, \tag{7}$$

is equal to $\langle \nu_{\mathrm{abs}} \rangle_{\mathrm{Al}} \approx 0.06$ for (π^+/K^+) Al and $\langle \nu_{\mathrm{abs}} \rangle_{\mathrm{Au}} \approx 0.25$ for (π^+/K^+) Au-interactions, thus corresponding to only 3–6% of $\langle \nu_T \rangle$. Note that in the charge balance $\langle Q \rangle$ they are multiplied by one (instead of Z/A), because in each $\pi'' d''$-absorption, the secondary charge changes by $(+1)$ (curve 4 in Fig. 11). The sums of the contributions of intranuclear collisions for π^+ and K^+ nuclei interactions are also shown in Fig. 11.

The calculations agree with the experimental data for the Al nucleus but the predicted Z-dependence is weaker than experimentally observed, probably due to the assumption that each target fragmentation product undergoes only one intranuclear collisions.

Table 5. Average multiplicities and cross sections of pions versus laboratory momentum

p_π (GeV/c)	< 0.2	0.2–0.4	0.4–0.9	0.9–2.5
$\bar{m}_\pi(p_\pi)$	~ 0.14	~ 0.43	~ 1.13	~ 1.3
$\bar{\sigma}_\pi(p_\pi)$	~ 15 mb	~ 60 mb	~ 25 mb	~ 30 mb

Table 6. Average multiplicities and cross sections of nucleons in two intervals of x_F

x_F	$x_F < -0.5$	$x_F > -0.5$
$\bar{m}_N(x_F)$	~ 0.47	~ 0.31
$\bar{\sigma}_N(x_F)$	~ 20 mb	~ 40 mb

6 The inelasticity coefficient

New information on the mechanisms of multiparticle production processes can be obtained from an investigation of another collective characteristic, i.c. the distribution of the total longitudinal momentum $\sum P_\parallel$ of charged particles in the beam fragmenation region ($y > 5$). These distributions are shown in Fig. 12; their first point

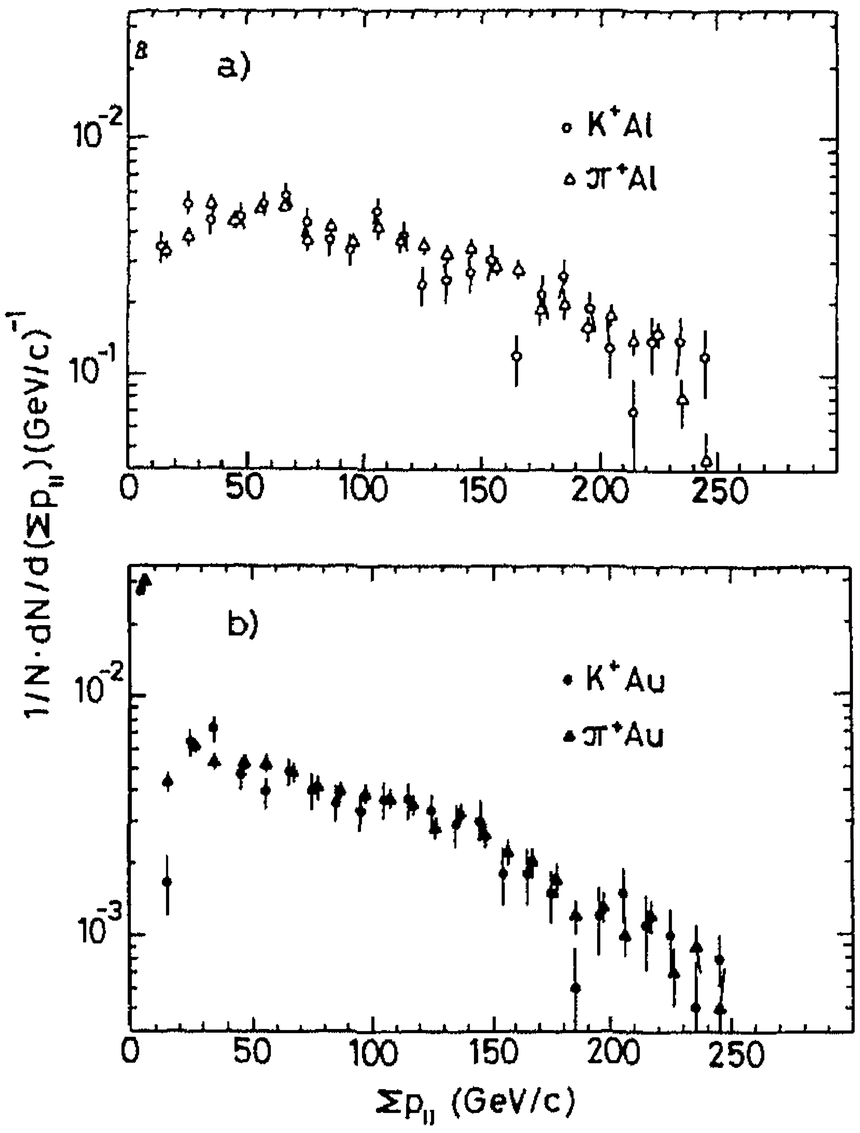

Fig. 12a, b. The distributions of the total longitudinal momentum $\sum P_{\|}$ of charged particles in the beam fragmentation region ($y > 5$)

($\sum P_{\|} = 0$) corresponds to events which do not contain charged particles with $y > 5$. The mean values of the quantity $\sum P_{\|}$ are:

$$\langle \sum P_{\|} \rangle_{\pi^+ \mathrm{Al}} = 81.5 \pm 1.2 \text{ GeV/c},$$

$$\langle \sum P_{\|} \rangle_{K^+ \mathrm{Al}} = 77.4 \pm 2.1 \text{ GeV/c},$$

$$\langle \sum P_{\|} \rangle_{\pi^+ \mathrm{Au}} = 68.1 \pm 1.1 \text{ GeV/c},$$

$$\langle \sum P_{\|} \rangle_{K^+ \mathrm{Au}} = 68.8 \pm 2.0 \text{ GeV/c}.$$

As expected, the average momentum losses for Au nuclei are larger than for Al:

$$r_{\pi^+} = \langle \sum P_{\|} \rangle_{\pi^+ \mathrm{Au}} / \langle \sum P_{\|} \rangle_{\pi^+ \mathrm{Al}} = 0.84 \pm 0.02,$$

$$r_{K^+} = \langle \sum P_{\|} \rangle_{K^+ \mathrm{Au}} / \langle \sum P_{\|} \rangle_{K^+ \mathrm{Al}} = 0.89 \pm 0.04.$$

Taking into account that the mean number of leading hadron (cluster) collisions in Au exceeds that in Al by about one unit (see Table 4), one can estimate the average momentum loss per collision (the inelasticity coefficient or the nuclear stopping power) to be approximately equal to $\bar{k} = 0.11$–0.16. This value agrees with an estimation [14] of the inelasticity coefficient $\bar{k} = 0.2 \pm 0.1$ for $\pi^+ p$ non-diffractive interactions, i.e. for the first inelastic interaction of the incident hadron in the nuclear medium. A more exact estimate of $\bar{k}$ can be obtained from the measured ratios r_{π^+} and r_{K^+}, in the framework of Glauber's multiple collision theory. If the hadron cluster produced in the first inelastic interaction of the incident hadron h carries on average $(1-\bar{k}_1)$ of the incident momentum P_0, and in each of the following collisions looses on average $\bar{k}$ of its longitudinal momentum, then one can show that the final longitudinal momentum of the cluster is equal to:

$$\langle P_{\|} \rangle = P_0 \frac{1-\bar{k}_1}{1-\bar{k}} \left[1 - \frac{\bar{k} N(0, \bar{k}\sigma^{\mathrm{in}}_{hN})}{N(0, \sigma^{\mathrm{in}}_{hN})} \right], \tag{8}$$

where $N(0, \sigma)$ is the so-called effective nuclear number (see (6)).

Figure 13 shows the ratio of momenta $\langle P_{\|} \rangle_{\mathrm{Au}} / \langle P_{\|} \rangle_{\mathrm{Al}}$ versus inelasticity $\bar{k}$ calculated by (8). Note that this ratio does not depend on $\bar{k}_1$. One can expect that this ratio is equal to the measured ratio $r_{\pi^+(K^+)}$ of the total longitudinal momentum of the fastest charged particles in the beam fragmentation. Then one can estimate from Fig. 13 the inelasticity coefficient: $\bar{k} = 0.18 \pm 0.03$ for π^+-nucleus and $\bar{k} = 0.14 \pm 0.06$ for K^+-nucleus interactions; its average value is $\bar{k} = 0.17 \pm 0.03$. Thus the important conclusion is obtained that the average inelasticity of hN-interactions is approximately the same as in the following inelastic collisions of the leading hadron cluster in nuclear matter; besides, the nuclear stopping powers for non-strange and strange clusters are approximately equal.

Some restrictions on the inelasticity coefficient can be obtained from the observed dependence of $\langle \sum P_{\|} \rangle$ on the number n_g of g-particles (Fig. 14) and on the summed

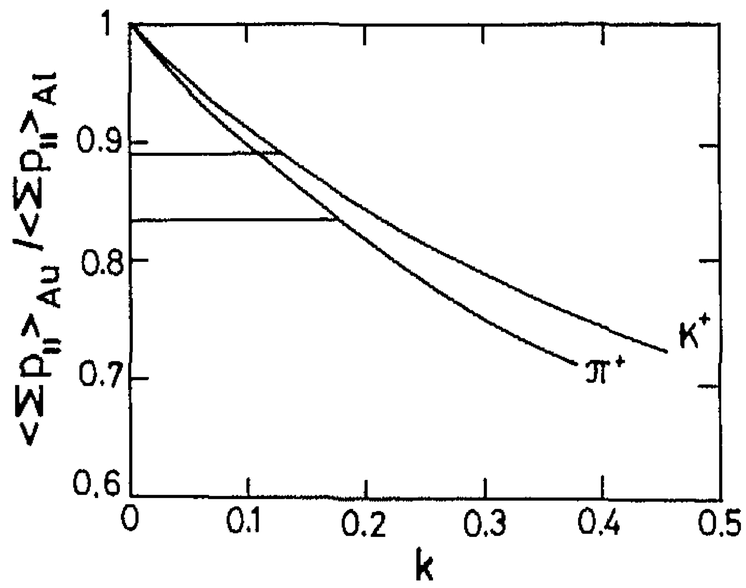

Fig. 13. The dependence of the ratio $\langle \sum P_{\|} \rangle_{\mathrm{Au}} / \langle \sum P_{\|} \rangle_{\mathrm{Al}}$ on the inelasticity coefficient $\bar{k}$

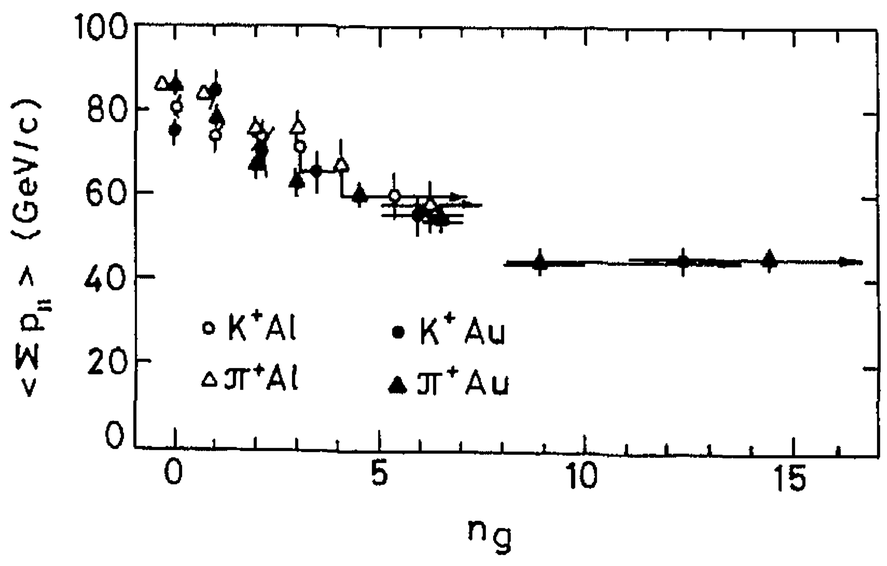

Fig. 14. The dependence of $\langle \sum P_{\|} \rangle$ on n_g

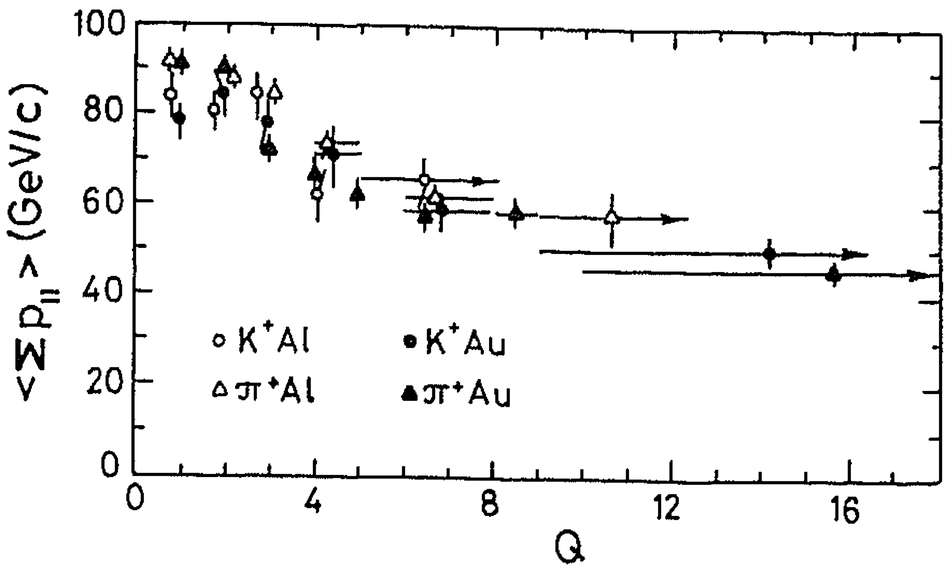

Fig. 15. The dependence of $\langle \sum P_{\parallel} \rangle$ on Q

charge of secondary particles Q (Fig. 15). As seen from Fig. 14 for peripheral interactions ($n_g = 0$ or 1), the total momentum $\langle \sum P_{\parallel} \rangle$ is about 80 GeV/c for (π^+/K^+) Al-interactions and decreases as n_g increases, reaching about 60 GeV/c for (π^+/K^+) Al-interactions (at $n_g \approx 6$) and about 45 GeV/c for (π^+/K^+) Au-interactions (at $n_g \approx 13$). Almost the same relative decrease of $\langle \sum P_{\parallel} \rangle$ is observed in its dependence on Q, which characterizes the number of intranuclear interactions: when one goes from peripheral interactions ($Q = 1$ or 2) to the most central ones ($Q \approx 10$ for Al and $Q \approx 15$ for Au), $\langle \sum P_{\parallel} \rangle$ decreases from 80 GeV/c to ~60 GeV/c for Al and to ~50 GeV/c for the Au nucleus.

Several models have been proposed [15, 16], which allow to express the correlation between the number of "grey" protons and the average number of leading hadron (cluster) collisions, $\langle \nu_A(n_g) \rangle$. For instance, for peripheral K^+ Au interactions ($n_g = 0$ or 1), $\langle \nu_A(n_g = 0\text{–}1) \rangle \approx 1.5$ in the model of Hegab and Hüfner [16], about 1.6 in the model of Andersson et al. and 1.8 if one uses the modified model [2] of Andersson et al. in which a negative binomial distribution of n_g for a single collision is used instead of the geometrical distribution proposed in [15]. For central K^+ Au interactions these models predict respectively the values $\langle \nu_A(\bar{n}_g = 12) \rangle = 6.0$, 4.9 and 4.3 (see [2]). Thus, on average, in the additional 2.5–4.5 collisions, the leading hadron (cluster) longitudinal momentum in K^+ Au-interactions degrades, as one can see from Fig. 14, by 44% (from 80 GeV/c to 45 GeV/c). If one assumes that the relative losses of momentum are the same in each collision, one obtains $\bar{k} = 0.15\text{–}0.20$, which is again in agreement with the estimated $\bar{k} = 0.2 \pm 0.1$ for elementary $\pi^+ p$ interactions at 250 GeV/c [14].

7 Summary

Multiparticle production processes are studied in K^+ Al, K^+ Au, π^+ Al and π^+ Au interactions at 250 GeV/c, based on a statistics of 9 K events.

New experimental data on the multiplicity distributions and inclusive spectra of protons and produced negative particles (essentially π^- mesons) are obtained.

The proton energy distributions for Al and Au nuclei are essentially similar, but the angular distributions demonstrate a strong A-dependence: the parameter α in the parametrization A^α for the proton average differential multiplicity is $\alpha = 0.42 \pm 0.02$ at very small angles and increases with increasing angle up to $\alpha = 0.73 \pm 0.03$ in the backward hemisphere at $\cos\theta < -0.3$, where its value becomes practically independent of θ.

A detailed study of the multiplication ratio R_- of negative particles is performed. The dependence of the average value of R_- on the average number of leading hadron (cluster) intranuclear collisions is obtained:

$$R_- = a + b\langle \nu_A \rangle ,$$

with $a = 0.70 \pm 0.14$, $b = 0.57 \pm 0.07$ and $a = 0.64 \pm 0.12$, $b = 0.50 \pm 0.06$ using the average $\langle n_- \rangle_{hp}$ in inelastic and in non-single diffractive hp-intractions, respectively.

It is shown that, in the target fragmentation region, R_- depends strongly on the number n_g of "grey" protons and reaches up to $R_- \sim 30\text{–}50$ for (π^+/K^+) Au interactions at small impact parameters. In the beam fragmentation region, the dependence on n_g disappears, and, at the largest rapidities, the multiplication ratio becomes less than one ($R_- = 0.37 \pm 0.06$ for π^+ Au and $R_- = 0.71 \pm 0.08$ for π^+ Al interactions).

By using the experimentally observed distributions of the total charge Q of the secondary particles, a model independent estimate for the average total number of intranuclear collisions is extracted and it is shown that their dominant part ($\simeq 60\%$ for Al and $\simeq 80\%$ for Au) is caused by interactions of the non-leading particles produced in the target fragmentation. The simplified calculations in the framework of Glauber theory agree with the measured value of $\langle Q \rangle$ for meson-Al interactions, but underestimate the $\langle Q \rangle$ for meson-Au intractions by about 25%, probably due to muliple collisions of secondary particles within the nucleus.

First experimental data on the total longitudinal momentum $\sum P_{\parallel}$ of charged particles produced in the beam fragmentation region ($y > 5$) are obtained. From comparison of data on Al and Au targets, the average inelasticity coefficient of the leading hadron (cluster) intranuclear interactions (or the nuclear stopping power) is extracted: $\bar{k} = 0.17 \pm 0.03$. From the n_g-dependence of $\langle \sum P_{\parallel} \rangle$ we obtained in a model dependent way, $\bar{k} = 0.15\text{–}0.20$. Both these estimations of $\bar{k}$ are consistent with the value $\bar{k} = 0.2 \pm 0.1$ found for $\pi^+ p$-interactions. Thus, in the intranuclear multiple collision process, the first and the following inelastic collisions occur with approximately the same inelasticity, which is similar also for non-strange and strange leading clusters.

Acknowledgements. It is a pleasure to thank the operating crews and staff of EHS and the H2 beam, as well as the scanning and measuring teams at our laboratories for the invaluable help with this experiments. The contributions of the Aachen, Helsinki and Warsaw groups to the earlier phase of this experiment are gratefully acknowledged.

References

1. S. Frederiksson, G. Eilam, G. Berlad, L. Bergström: Phys. Rep. 144 (1987) 188

2. M. Adamus et al., NA22: Z. Phys. C - Particles and Fields 42 (1989) 377
3. I.V. Ajinenko et al., NA22: Z. Phys. C - Particles and Fields 46 (1990) 569
4. M. Aguilar-Benitez et al.: Nucl. Instrum. Methods 205 (1983) 79
5. M. Adamus et al., NA22: Z. Phys. C - Particles and Fields 32 (1986) 475
6. M. Adamus et al. NA22: Z. Phys. C - Particles and Fields 39 (1988) 311
7. M. Adamus et al., NA22: Z. Phys. C - Particles and Fields 39 (1988) 301
8. A.S. Caroll et al.: Phys. Lett. 80B (1979) 319
9. C. DeMarzo et al., NA5: Phys. Rev. D26 (1982) 1019
10. J.E. Elias et al.: Phys. Rev. D22 (1980) 13
11. S.R. Gevorkyan, H.R. Gulkanyan, V.A. Vartanyan: Acta Phys. Pol. B15 (1984) 599
12. V. Flaminio et al.: CERN-HERA, 84-01, 1984
13. O. Taveras et al.: Lett. Nuovo Cimento 27 (1980) 358
14. I.V. Ajinenko et al., NA22: Z. Phys. C - Particles and Fields 49 (1991) 367
15. B. Andersson, I. Otterlund, E. Stenlund: Phys. Lett. 73B (1978) 343
16. M.K. Hegab, J. Hüfner: Nucl. Phys. A384 (1982) 353